

Processing of hydrocarbon dust in star-forming galaxies revealed with *AKARI*

AKINO KONDO,¹ HIDEHIRO KANEDA,¹ MISATO FUKAGAWA,¹ TOYOAKI SUZUKI,¹ KATSUHIRO L. MURATA,²
TAKUMA KOKUSHO,¹ AND SHINKI OYABU¹

¹Graduate School of Science, Nagoya University, Furo-cho, Chikusa-ku, Nagoya, Aichi, 464-8602, Japan

²Department of Physics, School of Science, Tokyo Institute of Technology, 2-12-1 Ohokayama, Meguro, Tokyo, 152-8551, Japan

ABSTRACT

Hydrocarbon dust is one of the dominant components of interstellar dust, which mainly consists of polycyclic aromatic hydrocarbons and aliphatic hydrocarbons. While hydrocarbon dust is thought to be processed in interstellar radiation fields or shocks, detailed processing mechanisms are not completely understood yet. Therefore, we study the infrared spectral properties of hydrocarbon dust for 138 pure star-forming galaxies at redshift $z < 0.3$. Using near-infrared spectra ($2.5\text{--}5\ \mu\text{m}$) obtained with *AKARI*/IRC, we derived the luminosities of the aromatic hydrocarbon feature at $3.3\ \mu\text{m}$ (L_{aromatic}) and the aliphatic hydrocarbon feature at $3.4\text{--}3.6\ \mu\text{m}$ ($L_{\text{aliphatic}}$). We also derived the total infrared luminosity (L_{IR}), the total PAH luminosity (L_{PAH}) and the radiation field strength by modeling the spectral energy distributions of the sample galaxies with *AKARI*, *IRAS*, and *WISE* photometry data. We find that $L_{\text{aliphatic}}/L_{\text{IR}}$ decreases with L_{IR} , like $L_{\text{PAH}}/L_{\text{IR}}$ shown in previous studies. Moreover, we find that $L_{\text{aliphatic}}/L_{\text{aromatic}}$ decreases with L_{IR} , indicating that aliphatic hydrocarbons are more highly processed than aromatic hydrocarbons. In this paper, we discuss possible processing mechanisms of interstellar hydrocarbon dust in galaxies with higher L_{IR} .

Keywords: infrared: ISM, galaxies: star formation, ISM: dust

1. INTRODUCTION

Hydrocarbon dust is one of the most important components of interstellar dust. Their smallest forms are known as polycyclic aromatic hydrocarbons (PAHs). PAHs contain benzene rings composed of 50–100 carbon atoms. The presence of PAHs is often identified through near- to mid-infrared spectral features (Tielens 2008; Peeters et al. 2002). For example, Spitzer/IRS covers the mid-infrared spectral features, while *AKARI*/IRC covers the near-infrared spectral features. From near-infrared spectra of star-forming galaxies, *AKARI*/IRC detected a strong emission feature at $3.3\ \mu\text{m}$ due to an aromatic component. *AKARI* also detects the emission features of aliphatic components at $3.4\text{--}3.6\ \mu\text{m}$. These emission features are both produced by a C–H stretching mode.

Many previous studies have investigated the properties of PAHs in star-forming galaxies. Desai et al. (2007) found that $L_{\text{PAH}}/L_{\text{IR}}$ decreases with increasing L_{IR} using the mid-infrared features. Imanishi et al. (2010) and Yamada et al. (2013) obtained a similar trend using the near-infrared features. Yamada et al. (2013) showed that $L_{\text{aromatic}}/L_{\text{IR}}$ decreases with L_{IR} for 101 star-forming galaxies and concluded that the relative abundance of PAHs is decreased in galaxies with higher L_{IR} . There are two possible major channels through which PAHs are destroyed; one is the photodissociation in strong radiation fields, and the other is the large-scale shocks induced by galaxy merger. Murata et al. (2017) suggested that both are comparably important for the destruction of PAHs. However, these previous studies have investigated only the aromatic features. Therefore, we study the aliphatic feature of star-forming galaxies and its relationship with the aromatic feature to understand the detailed processing mechanism of hydrocarbon dust.

2. DATA ANALYSIS

We analyzed the *AKARI* spectra of 230 mid-infrared excess galaxies at redshift $z < 0.3$. These sources were selected based on the *AKARI* mid-infrared all-sky surveys with the criteria that the flux ratio of 9 or 18 to $2.2\ \mu\text{m}$ is larger than 2. Then, near-infrared follow-up spectroscopy of these sources was performed with *AKARI*/IRC. From the near-infrared spectra, we classified these galaxies into three types; pure star-forming galaxies, pure AGNs, and composite galaxies with

star-formation and AGN based on the presence of star formation activity and AGN activity. The star formation activity was judged by the equivalent width of the $3.3\ \mu\text{m}$ aromatic feature, $\text{EW}_{3.3\ \mu\text{m}}$. In this study, the star formation is considered to be active in the case of $\text{EW}_{3.3\ \mu\text{m}} > 40\ \text{nm}$ (Moorwood 1986; Imanishi & Dudley 2000; Imanishi et al. 2008). The AGN activity was judged by the near-infrared continuum slope, Γ ($F_{\text{continuum}} \propto \lambda^\Gamma$). In this study, the contribution of AGN is considered to be non-negligible in the case of $\Gamma > 1$ (Risaliti et al. 2006; Imanishi et al. 2010). As a result, our sample contains 138 pure star-forming galaxies, 57 pure AGNs, and 35 composite galaxies. We discuss only pure star-forming galaxies in this paper.

After sample selection, we performed spectral fitting to the near-infrared spectra. The left panel of Figure 1 shows an example of the spectral fitting results for the star-forming galaxies. In order to investigate the hydrocarbon features, we took into account the following components in our fitting model: H_2O ice, aromatic feature, aliphatic feature, and near-infrared continuum. Thus, the total flux density of the spectrum is defined as

$$F_\nu = e^{-\tau}(F_{\text{continuum}} + F_{\text{aromatic}} + F_{\text{aliphatic}}), \quad (1)$$

where τ is the optical depth caused by the H_2O ice absorption, and $F_{\text{continuum}}$, F_{aromatic} and $F_{\text{aliphatic}}$ are the flux density of each component. We simply assumed the full screen geometry as a source of τ . We used a Lorentzian profile for the H_2O ice feature, a Drude profile for the aromatic feature, a Lorentzian or Gaussian profile for the aliphatic features, and power-law for the near-infrared continuum. Finally, we calculated the luminosity of the aromatic and aliphatic feature (L_{aromatic} , $L_{\text{aliphatic}}$) from the result of the spectral fitting.

In addition to the spectral fitting, we also performed SED fitting. The right panel of Figure 1 shows an example of the SED fitting results for the star-forming galaxies. We used mid- to far-infrared photometric data with *AKARI*, *WISE* and *IRAS*. Moreover, we also used the binned spectral data points of the above *AKARI*/*IRC* near-infrared spectra in order to reproduce the near-infrared stellar continuum. The SED model is based on the DustEM code (Compiègne et al. 2011). Hence, the total flux density includes the four dust components; PAH, very small grain, big grain and stellar continuum. From the SED fitting, we obtained the total infrared luminosity (L_{IR}) and the UV radiation field intensity indicated by G_0 (Habing 1968).

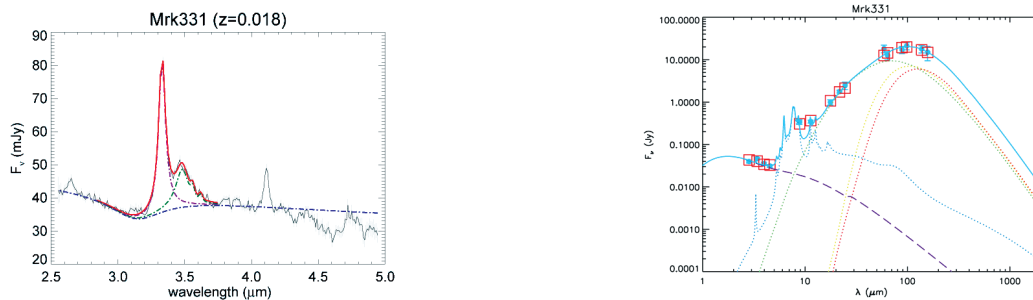


Figure 1. (left) Spectral fitting result for the star-forming galaxy Mrk 331. The observed spectrum is shown as black solid line. The spectral model is composed of the near-IR continuum (blue dot-dashed line), the aromatic hydrocarbon (magenta dot-dashed line) and aliphatic hydrocarbon features (green dot-dashed line). These components are influenced by the H_2O ice absorption. The total model spectrum is shown as red solid line. (right) SED fitting result for the star-forming galaxy Mrk 331. The observed SEDs are shown as cyan filled circle. The SED model is composed of ionized PAH (blue dotted line), neutral PAH (purple dotted line), small amorphous carbon dust (green dotted line), large amorphous carbon dust (yellow dotted line), amorphous silicate dust (red dotted line), and near-IR continuum (purple dashed line). The total model spectrum and the model flux densities are shown as cyan solid line and red square, respectively.

3. RESULTS

We investigated the relationship between the PAH and total infrared luminosities for each of the sample galaxies. Figure 2 displays the distributions of $L_{\text{aromatic}}/L_{\text{IR}}$ for the infrared galaxies (IRGs: $L_{\text{IR}} < 10^{11} L_{\odot}$), luminous infrared galaxies (LIRGs: $10^{11} L_{\odot} < L_{\text{IR}} < 10^{12} L_{\odot}$) and ultra-luminous infrared galaxies (ULIRGs: $L_{\text{IR}} > 10^{12} L_{\odot}$). The histograms show that $L_{\text{aromatic}}/L_{\text{IR}}$ systematically decreases with L_{IR} , which confirms the results of Yamada et al. (2013). As a new result, we find that not only the aromatic feature but also the aliphatic feature is correlated with L_{IR} . Figure 3 displays the distributions of $L_{\text{aliphatic}}/L_{\text{IR}}$ for the IRGs, LIRGs and ULIRGs. The histograms show that $L_{\text{aliphatic}}/L_{\text{IR}}$ systematically changes with L_{IR} , similarly to the trend of $L_{\text{aromatic}}/L_{\text{IR}}$. These results suggest that the relative abundances of aromatic and aliphatic hydrocarbons may be related to each other.

Moreover, Figure 4 shows the distributions of $L_{\text{aliphatic}}/L_{\text{aromatic}}$ for the IRGs, LIRGs and ULIRGs. $L_{\text{aliphatic}}/L_{\text{aromatic}}$ shows a decreasing trend with a large scatter at higher L_{IR} . From these results, we find that $L_{\text{aliphatic}}/L_{\text{aromatic}}$ as well as $L_{\text{aromatic,aliphatic}}/L_{\text{IR}}$ decreases with increasing L_{IR} . Therefore, PAHs tend to become aromatic-rich, while they are being destroyed in galaxies with higher L_{IR} .

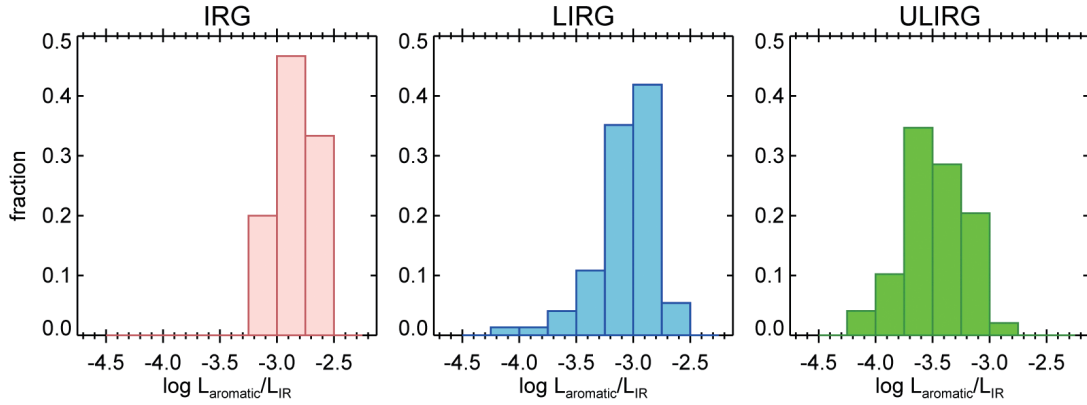


Figure 2. Distributions of $L_{\text{aromatic}}/L_{\text{IR}}$ for the IRGs, LIRGs and ULIRGs of our sample.

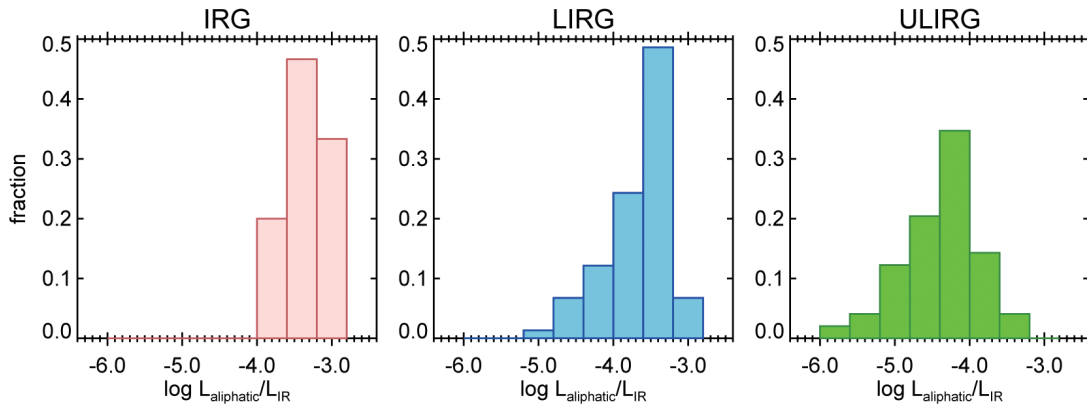


Figure 3. Distributions of $L_{\text{aliphatic}}/L_{\text{IR}}$ for the IRGs, LIRGs and ULIRGs of our sample.

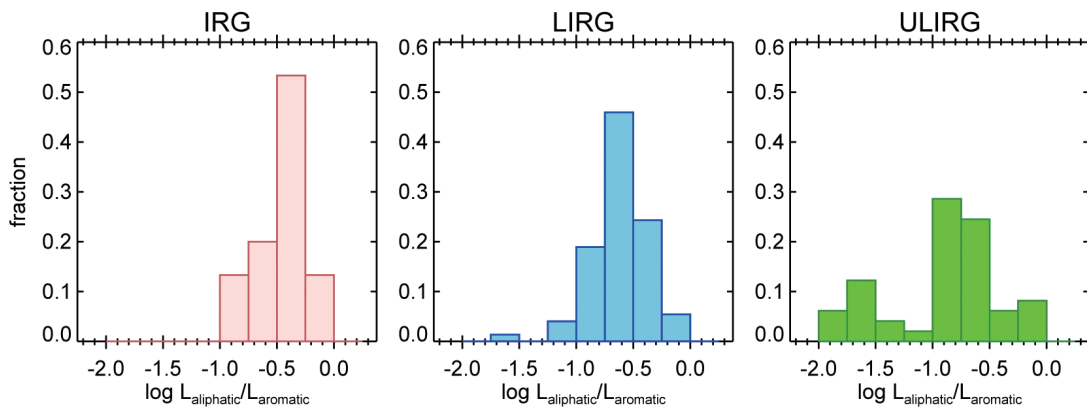


Figure 4. Distributions of $L_{\text{aliphatic}}/L_{\text{aromatic}}$ for the IRGs, LIRGs and ULIRGs of our sample.

4. DISCUSSION

In order to investigate whether or not the variations of $L_{\text{aliphatic}}/L_{\text{aromatic}}$ are really intrinsic, we evaluate the effect of the presence of the absorption feature due to carbonaceous dust. We assume that the optical depth of carbonaceous dust, $\tau_{3.4\mu\text{m}}$ correlates with the optical depth of H₂O ice, $\tau_{3.1\mu\text{m}}$. We consider that $\tau_{3.4\mu\text{m}}/\tau_{3.1\mu\text{m}}$ is 0.38–0.85 as derived from the AKARI observations of dusty AGNs (Imanishi et al. 2010). Under these assumptions, we estimate $\tau_{3.4\mu\text{m}}$ from the measured $\tau_{3.1\mu\text{m}}$ and investigate how $L_{\text{aliphatic}}/L_{\text{aromatic}}$ declines. The left panel of Figure 5 shows the relationship between $L_{\text{aliphatic}}/L_{\text{aromatic}}$ and $\tau_{3.1\mu\text{m}}$. As can be seen in the figure, the carbonaceous dust absorption cannot change

$L_{\text{aliphatic}}/L_{\text{aromatic}}$ by a factor larger than 10. This result rules out a possibility that the carbonaceous dust absorption is a main cause of the decrease in $L_{\text{aliphatic}}/L_{\text{aromatic}}$. Therefore, we verify that $L_{\text{aliphatic}}/L_{\text{aromatic}}$ is intrinsically variable.

We discuss the processing mechanism of the hydrocarbon dust. First, we evaluate the effect of the strong radiation field using G_0 derived from the SED fitting. The right panel of Figure 5 shows $L_{\text{aliphatic}}/L_{\text{aromatic}}$ plotted against G_0 . All the galaxies with very low $L_{\text{aliphatic}}/L_{\text{aromatic}}$ show G_0 larger than 30, indicating that there is a threshold on G_0 . The threshold on G_0 suggests that the strong radiation fields are likely to cause the decrease in $L_{\text{aliphatic}}/L_{\text{aromatic}}$, since aliphatic bonds are known to be chemically weaker than aromatic bonds against photodissociation. However, the figure also shows a large scatter of $L_{\text{aliphatic}}/L_{\text{aromatic}}$ at G_0 larger than 30, which cannot be explained by G_0 alone.

Based on the galaxy morphology in the SDSS g -band or the HST F814W image, we classified our sample into the following three types; non-merger galaxies, early stage merger galaxies and late stage merger galaxies (Murata et al. 2017). The difference in the symbol in the right panel of Figure 5 corresponds to the difference in the galaxy merger type. At G_0 larger than 30, late stage merger galaxies tend to show low $L_{\text{aliphatic}}/L_{\text{aromatic}}$. This result suggests that difference in the merger stage may contribute to the large scatter of $L_{\text{aliphatic}}/L_{\text{aromatic}}$.

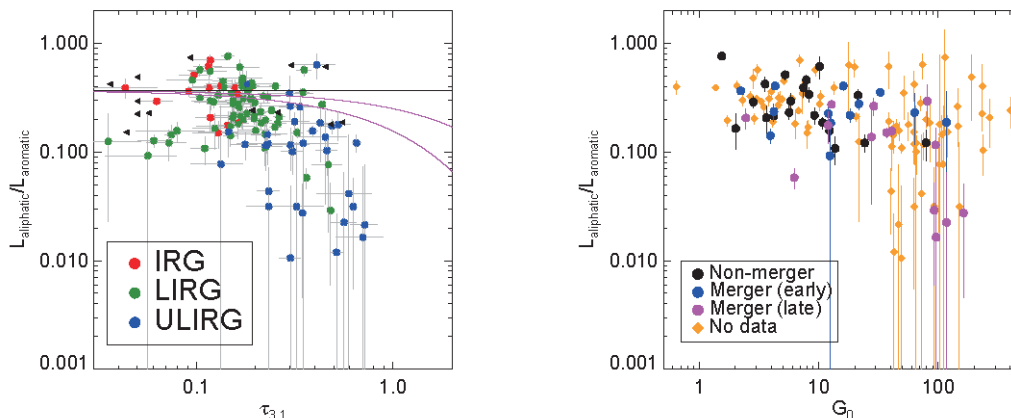


Figure 5. (left) $L_{\text{aliphatic}}/L_{\text{aromatic}}$ plotted against $\tau_{3.1\mu\text{m}}$ for the star-forming galaxies; the IRGs (red circles), the LIRGs (green circles) and the ULIRGs (blue circles). The black dashed line shows the mean value of $L_{\text{aliphatic}}/L_{\text{aromatic}}$ for the IRGs and the magenta dot-dashed line shows the values which consider the carbonaceous dust absorption. (right) $L_{\text{aliphatic}}/L_{\text{aromatic}}$ plotted against G_0 where different symbols are used for different galaxy merger types; non-merger galaxies (black circles), early stage merger galaxies (blue circles) and late stage merger galaxies (magenta circles). Orange diamonds show galaxies which were not observed by SDSS or HST.

5. SUMMARY

We have systematically studied the behavior of the aliphatic to aromatic ratios for pure star-forming galaxies in order to investigate the processing mechanism of hydrocarbon dust. Specifically, we selected 138 pure star-forming galaxies and performed near-infrared spectral fitting and near- to far-infrared SED fitting. As a result, we find that $L_{\text{aliphatic}}/L_{\text{IR}}$ decreases with L_{IR} , similarly to $L_{\text{PAH}}/L_{\text{IR}}$ as shown in the previous studies. Moreover, we find that $L_{\text{aliphatic}}/L_{\text{aromatic}}$ decreases with L_{IR} and verify that the variations of $L_{\text{aliphatic}}/L_{\text{aromatic}}$ is intrinsic. Our study suggests that PAHs become aromatic-rich while they are being processed through strong radiation fields at late stage merger galaxies.

REFERENCES

- Compiègne, M., Verstraete, L., Jones, A., et al. 2011, *A&A*, 525, A103
 Desai, V., Armus, L., Spoon, H. W. W., et al. 2007, *ApJ*, 669, 810
 Habing H. J., 1968, *Bull. Astron. Inst. Netherlands*, 19, 421
 Imanishi, M., & Dudley, C. C. 2000, *ApJ*, 545, 701
 Imanishi, M., Nakagawa, T., Ohya, Y., et al. 2008, *PASJ*, 60, S489
 Imanishi, M., Nakagawa, T., Shirahata, M., Ohya, Y., Onaka, T., 2010, *ApJ*, 721, 1233
 Moorwood, A. F. M. 1986, *A&A*, 166, 4
 Murata, K. L., Yamada, R., Oyabu, S., et al. 2017, *MNRAS*, 472, 39
 Peeters, E., Hony, S., Van Kerckhoven, C., et al. 2002, *A&A*, 390, 1089
 Risaliti, G., Maiolino, R., Marconi, A., et al. 2006, *MNRAS*, 365, 303
 Tielens, A. G. G. M. 2008, *ARA&A*, 46, 289
 Yamada, R., Oyabu, S., Kaneda, H., et al. 2013, *PASJ*, 65, 103